Eur. Phys. J. C (2025) 85:431
https://doi.org/10.1140/epjc/s10052-025-14174-1

THE EUROPEAN PHYSICAL JOURNAL C

Regular Article - Theoretical Physics

Black hole shadows in accelerating Kerr–Newman–Taub–NUT and Braneworld spacetimes

Haryanto M. Siahaan[a]

Program Studi Fisika, Universitas Katolik Parahyangan, Jalan Ciumbuleuit 94, Bandung 40141, Indonesia

Received: 25 February 2025 / Accepted: 8 April 2025

Abstract We investigate the null geodesic structure and corresponding black hole shadows in the accelerating Kerr–Newman–Taub–NUT (AKNTN) spacetime-a highly generalized solution that incorporates rotation, electric charge, acceleration, and NUT charge. By deriving a separable Hamilton–Jacobi equation for null test particles, we demonstrate that the additional parameters enable equatorial circular photon orbits, a feature absent in generic accelerating spacetimes. Building on this framework, we analyze the influence of acceleration, spin, electric (or tidal) charge, and NUT parameters on the shadow observables, such as the shadow radius and distortion. Furthermore, we extend our study to include tidal charged black holes in the RS-II braneworld scenario by replacing the electric charge parameter with a tidal charge, $\mathcal{Q}$, which may assume either sign. Our numerical results reveal that increasing the acceleration parameter compresses the photon capture region and reduces the shadow size, while a negative tidal charge deepens the gravitational potential, enlarging the shadow. These findings offer new insights into the interplay between extra-dimensional effects and classical gravitational parameters, with potential implications for future astrophysical observations.

1 Introduction

Over recent decades, the accelerating Taub–NUT spacetime has garnered significant attention and been the focus of extensive research [1–11]. In [6], a compact and elegant formulation of the accelerating Taub–NUT metric was introduced, which was subsequently generalized to include rotation and electric charge in [7]. Further developments, such as incorporating a cosmological constant, were presented in [8], and an optimized representation of the accelerating and rotating Taub–NUT spacetime was provided in [9]. These advancements highlight the pivotal role of the accelerating Taub–NUT solution in deepening our understanding of Einstein's theory of gravity. Specifically, the metric described in [6] solves the vacuum Einstein field equations, whereas its electrically charged generalization aligns with the Einstein–Maxwell framework [7,9].

A key feature of black holes that continues to captivate researchers is the phenomenon of black hole shadows. It is well understood that null geodesics around a black hole can result in three distinct outcomes: absorption by the black hole, stable orbits around it, or reflection to infinity. These dynamics manifest as a dark region, or shadow, observable by a distant observer at a fixed coordinate position [12–16].

Shadows are not limited to the charged and rotating black holes; they can also be exhibited by accelerating ones [17]. Moreover, lensing phenomena associated with accelerating black holes have been investigated in [18,19]. These studies reflect the scientific curiosity to explore a broad range of spacetime parameters arising from exact solutions to Einstein's equations, including the acceleration parameter present in the C-metric [20]. Recent examples on investigations into black hole shadows, employing approaches similar to those adopted in this paper, can be summarized as follows. In [21], the shadow of a novel black hole solution in Einstein gravity, incorporating Ayon–Beato–Garcia nonlinear electrodynamics and a cloud of strings, was analyzed. The shadow of rotating black holes within the framework of bumblebee gravity was studied in [22]. An intriguing development is presented in [23], where shadow observations of Sgr A* were used to constrain the NUT charge. Gravitational lensing and shadow effects around a Schwarzschild-like black hole in metric-affine bumblebee gravity were examined in [24], while [25] explored light rings and shadows of

[a] e-mail: haryanto.siahaan@unpar.ac.id (corresponding author)

Published online: 17 April 2025

static black holes using the Hamiltonian constraint approach to effective quantum gravity.

Recently, a more generalized solution describing a rotating, accelerating, and charged black hole with NUT charge in the Einstein–Maxwell theory was developed [6–8]. This solution extends the Plebański–Demiański family [20,26], incorporating NUT and acceleration parameters alongside those of the Kerr–Newman solution. Its neutral limit has been employed in [27] to construct the heterotic string theory counterpart of an accelerating charged and rotating Taub–NUT black hole, while the corresponding Kerr/CFT correspondence has been studied in [28].

The study of black hole spacetimes in modified gravity frameworks has opened new avenues for understanding gravitational phenomena beyond general relativity. Among these frameworks, the RS-II braneworld scenario offers a compelling approach, wherein the effects of the bulk spacetime manifest as corrections to the effective Einstein equations on the brane. A notable consequence of this scenario is the emergence of tidal charges, which serve as observable imprints of the extra-dimensional influences [29–32]. By assuming the existence of the effective stress-energy tensor which comes from the bulk effect, one can show that electrically charged black hole solutions in Einstein–Maxwell theory can be associated to some tidal charged black holes on the 3-brane in RS-II scenario [30,33], including the spacetime solution discussed in this work.

In this paper, we aim to analyze the shadow of the accelerating Kerr–Newman–Taub–NUT (AKNTN) black hole. Previous work [17] demonstrated that black hole acceleration prevents the existence of circular photon orbits confined to a fixed equatorial plane. This raises an interesting question: could the inclusion of additional parameters, such as electric charge and NUT charge, enable such orbits? To address this, we first establish a separable Hamilton–Jacobi equation for null geodesics. The shadow of the AKNTN black hole is then studied using the methods described in [12,34]. Furthermore, the discussions can be extended to the tidal charged black hole in RS-II braneworld scenario.

The structure of this paper is as follows. In the next section, we discuss the null orbits in AKNTN spacetime. In the next section, we study some aspects of AKNTN spacetime including the Hamilton–Jacobi and null orbits. Section 3 investigates the shadow of the AKNTN black hole using the approach outlined in [12]. Section 4 explores the extension of the AKNTN solution to a braneworld scenario [7], along with an analysis of the associated black hole shadow. The observables derived from the black hole shadow are presented in Sect. 5, following the methodology in [34]. Finally, we conclude with a summary of our findings and future possible works. Throughout this paper, we consider the unit speed of light and Newton's gravitational constant, $c = G = 1$.

2 Some aspects of accelerating Kerr–Newman–Taub–NUT spacetime

The accelerating Kerr–Newman–Taub–NUT (AKNTN) spacetime is an extensively generalized solution to the Einstein–Maxwell equations, integrating rotation, electric charge, acceleration, and gravitomagnetic (NUT) effects into a single metric. As a distinguished member of the broader Plebański–Demiański class, this solution is characterized by a nontrivial conformal factor that drives the acceleration, thereby giving rise to unique features such as additional (acceleration) horizons and conical singularities, which may be interpreted as cosmic strings or struts. In this section, we present the explicit form of the AKNTN metric along with its associated vector potential, examine its curvature invariants, and derive the equations governing null geodesics. This analysis not only elucidates the intricate interplay among the various spacetime parameters but also offers essential insights into observable phenomena, such as the black hole shadow, which will be discussed in the following section.

The spacetime solution describing an accelerating Kerr–Newman–Taub–NUT (AKNTN) spacetime is given by [7]

$$\mathrm{d}s^2 = \frac{1}{\Omega^2}\left\{-\frac{\Delta_r}{\Sigma}\left(\mathrm{d}t - Z_\theta \mathrm{d}\phi\right)^2 + \frac{\Sigma}{\Delta_r}\mathrm{d}r^2 + \frac{\Sigma}{P}\mathrm{d}\theta^2 + \frac{P\sin^2\theta}{\Sigma}\left(a\mathrm{d}t - Z_r\mathrm{d}\phi\right)^2\right\}, \tag{2.1}$$

where

$$\Omega = 1 - \frac{bar\,(n + a\cos\theta)}{a^2 + n^2}, \tag{2.2}$$

$$\Delta_r = (r - r_+)(r - r_-)\left(1 + \frac{bar\,(a - n)}{a^2 + n^2}\right) \times \left(1 - \frac{bar\,(a + n)}{a^2 + n^2}\right), \tag{2.3}$$

$$P = \left(1 - \frac{bar_+\,(a + n\cos\theta)}{a^2 + n^2}\right) \times \left(1 - \frac{bar_-\,(a + n\cos\theta)}{a^2 + n^2}\right), \tag{2.4}$$

$$\Sigma = r^2 + (n + a\cos\theta)^2, \tag{2.5}$$

$$Z_r = r^2 + (a + n)^2, \tag{2.6}$$

and

$$Z_\theta = a\sin^2\theta + 2n\,(1 - \cos\theta). \tag{2.7}$$

The accompanying vector solution is

$$A_\mu \mathrm{d}x^\mu = \frac{qr}{\Sigma}\left[\mathrm{d}t + \left(a\sin^2\theta + 2n\,(1 - \cos\theta)\right)\mathrm{d}\phi\right] \tag{2.8}$$

Together with the metric (2.1), these vector fields obey the equations of motion in Einstein–Maxwell theory, i.e.

$$R_{\mu\nu} = 2F_{\mu\alpha}F_{\nu\beta}g^{\alpha\beta} - \frac{1}{2}g_{\mu\nu}F_{\alpha\beta}F^{\alpha\beta}, \tag{2.9}$$

and the source-free condition $\nabla_\mu F^{\mu\nu} = 0$. From the metric function in Eq. (2.1), the location of black hole horizons are given by $r_\pm = m \pm \sqrt{m^2+n^2-a^2-q^2}$. In addition to the black hole horizons, the AKNTN spacetime also features accelerating horizons, governed by the Ω function in Eq. (2.1). However, a comprehensive discussion of the rich structure of the AKNTN spacetime is beyond the scope of this work. For further details, readers are encouraged to refer to Refs. [6–8].

A typical quantity to learn about the geometry of spacetime is the squared Riemann tensor or Kretchmann scalar. NUTty spacetime is known for its property where the true singularity at origin is absent, replaced by semi-infinite or infinite string-like singularity on the rotational axis. To distinguish the accelerating NUTty spacetime as one discussed in this paper to its non-accelerating counterpart, let us examine the Kretchmann scalar associates to the AKNTN spacetime. Since we like to contrast the spacetime property between the one with and without acceleration parameter for NUTty spacetime, we can simply consider the electrically neutral case of the spacetime metric (2.1). In fact, such consideration reduces the complexity of resulting mathematical expression significantly for the Kretchmann scalar.

$$C \equiv R_{\alpha\beta\mu\nu}R^{\alpha\beta\mu\nu} = -\frac{28\left(a^2+n^2-barN\right)^6 C_+C_-}{\left(a^2+n^2\right)\Sigma^3}, \tag{2.10}$$

where

$$\begin{aligned}
C_+ = &\left(\left(a^2+abn^2+n^2-a^3b\right)m+n^3+ba^3n\right.\\
&\left.+na^2-ban^3\right)r^3\\
&-3N\left(ba^3n+a^3bm-na^2+a^2m-ban^3\right.\\
&\left.-ambn^2+mn^2-n^3\right)r^2\\
&-3N^2\left(ambn^2+mn^2+na^2+a^2m+n^3\right.\\
&\left.+ba^3n-ban^3-a^3bm\right)r\\
&+N^3\left(ba^3n+a^3bm-na^2+a^2m-ban^3\right.\\
&\left.-ambn^2+mn^2-n^3\right),
\end{aligned} \tag{2.11}$$

and

$$\begin{aligned}
C_- = &\left(\left(abn^2-n^2-a^3b-a^2\right)m+l^3+bal^3\right.\\
&\left.+la^2-ba^3l\right)r^3\\
&-3N\left(ambn^2+mn^2+na^2+a^2m+n^3+ba^3n\right.\\
&\left.-ban^3-a^3bm\right)r^2\\
&+3N^2\left(ba^3n+a^3bm-na^2+a^2m-ban^3\right.\\
&\left.-ambn^2+mn^2-n^3\right)r\\
&+N^3\left(ambn^2+mn^2+na^2+a^2m+n^3\right.\\
&\left.+ba^3n-ban^3-a^3bm\right),
\end{aligned} \tag{2.12}$$

where $N = n + a\cos\theta$. Interestingly, at origin this quantity takes the form

$$\begin{aligned}
C_0 = \lim_{r\to 0} C = &\frac{48}{\left(a^2+n^2\right)^2N^6}\left(a^3bm-ba^3n\right.\\
&-a^2n-a^2m+ban^3-ambn^2-n^3\\
&\left.-mn^2\right)\left(a^3bm+ba^3n+a^2m-a^2n-ambn^2\right.\\
&\left.-ban^3-n^3+mn^2\right),
\end{aligned} \tag{2.13}$$

which hints the existence of ring singularity just like in the case of Kerr black hole. Taking the non-rotating limit in the last expression shows the typical property of spacetime with the NUT parameter, where an accelerating NUTty spacetime does not possess the true singularity at origin. To help the readers in understanding this quantity, numerical evaluations of C are given in Fig. 1.

Now let us start to study the motion of null objects in AKNTN spacetime. To do so, we consider the test object with general Lagrangian

$$\mathcal{L} = \frac{1}{2}g_{\mu\nu}\frac{dx^\mu}{d\sigma}\frac{dx^\nu}{d\sigma}, \tag{2.14}$$

where σ is some affine parameters. The energy and angular momentum of the object is given by

$$\begin{aligned}
-E = g_{t\mu}\frac{dx^\mu}{d\sigma} = &-\left(\frac{\Delta_r - P\sin^2\theta a^2}{\Omega^2\Sigma}\right)\frac{dt}{d\sigma}\\
&+\left(\frac{\Delta_r Z_\theta - P\sin^2\theta a Z_r}{\Omega^2\Sigma}\right)\frac{d\phi}{d\sigma},
\end{aligned} \tag{2.15}$$

and

$$\begin{aligned}
L = g_{\phi\mu}\frac{dx^\mu}{d\sigma} = &\left(\frac{\Delta_r Z_\theta - P\sin^2\theta a Z_r}{\Omega^2\Sigma}\right)\frac{dt}{d\sigma}\\
&+\left(\frac{P\sin^2\theta a Z_r^2 - \Delta_r {Z_\theta}^2}{\Omega^2\Sigma}\right)\frac{d\phi}{d\sigma}.
\end{aligned} \tag{2.16}$$

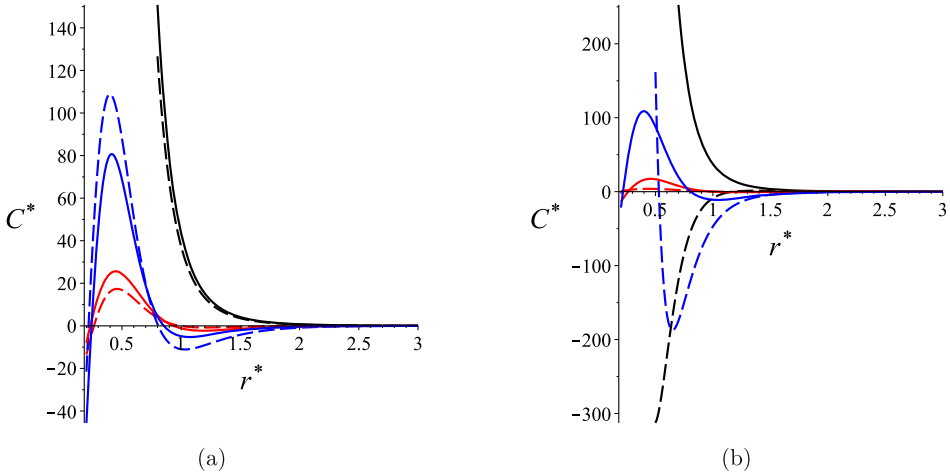

Fig. 1 Dimensionless Kretchmann scalar, $C^* = Cm^4$, varying with respect to radius $r^* = r/m$ for accelerating Kerr–Taub–NUT spacetime, namely $q = 0$ case. Black, red, and blue plots correspond to the $\theta = \pi/2$, $\theta = 0$, and $\theta = \pi$ cases, respectively. In **a**, the dashed plots represent the $bm = 0.1$ case, whereas solid ones correspond to the non-accelerating case, and we have considered $a = 0.9m$ and $n = 0.1m$. In **b**, the plots represent the $n = 0.5m$ case, whereas solid ones correspond to the $n = 0.1m$ case. Here we consider $a = 0.9m$ and $bm = 0.1$

Accordingly,

$$\frac{d\phi}{d\sigma} = \frac{\Omega^2 \left\{ \left(\Delta_r - P\sin^2\theta a^2 \right) L - \left(\Delta_r Z_\theta - P\sin^2\theta a Z_r \right) E \right\}}{\Sigma \sin^2\theta \Delta_r P}, \tag{2.17}$$

and

$$\frac{dt}{d\sigma} = \frac{\Omega^2 \left\{ \left(\Delta_r Z_\theta - P\sin^2\theta a Z_r \right) L - \left(\Delta_r {Z_\theta}^2 - P\sin^2\theta Z_r^2 \right) E \right\}}{\Sigma \sin^2\theta \Delta_r P}. \tag{2.18}$$

It turns out that the spacetime (2.1) possesses the ∂_t and ∂_ϕ Killing symmetries. It yields we are allowed to employ the ansatz

$$S = -Et + L\phi + S_r(r) + S_\theta(\theta), \tag{2.19}$$

as the Hamilton–Jacobi equation for null test object $\partial_\mu S \partial^\mu S = 0$ can be expressed as

$$\begin{aligned} &P\left(\frac{dS_\theta}{d\theta}\right)^2 + \Delta_r \left(\frac{dS_r}{dr}\right)^2 + \frac{\left(\Delta_r Z_\theta^2 - P\sin^2\theta Z_r^2\right)}{\sin^2\theta \Delta_r P} E^2 \\ &+ \frac{\left(\Delta_r - P\sin^2\theta a^2\right)}{\sin^2\theta \Delta_r P} L^2 \\ &- \frac{2\left(\Delta_r Z_\theta - P\sin^2\theta a Z_r\right)}{\sin^2\theta \Delta_r P} EL = 0. \end{aligned} \tag{2.20}$$

Note that the conformal factor Ω does not contribute to the Hamilton–Jacobi equation above. Quite interestingly, despite the complexity of the spacetime metric (2.1), the Hamilton–Jacobi for null test objects above is separable, namely it can be separated into two equations

$$\Delta_r \left(\frac{dS_r}{dr}\right)^2 - \frac{(aL - Z_r E)^2}{\Delta_r} = -K, \tag{2.21}$$

and

$$P\left(\frac{dS_\theta}{d\theta}\right)^2 + \frac{(L - Z_\theta E)^2}{P\sin^2\theta} = K, \tag{2.22}$$

for some constants K. Thence, from the relation

$$\frac{\partial S}{\partial x^\mu} = g_{\mu\nu}\frac{dx^\nu}{d\sigma} \tag{2.23}$$

we can get

$$\frac{\Sigma}{\Omega^2}\frac{\mathrm{d}\theta}{\mathrm{d}\sigma} = \left[P\left(K + (L - aE)^2\right) - \frac{(L - Z_\theta E)^2}{\sin^2\theta} \right]^{1/2}, \tag{2.24}$$

and

$$\frac{\Sigma}{\Omega^2}\frac{\mathrm{d}r}{\mathrm{d}\sigma} = \left[(aL - Z_r E)^2 - \left(K + (L - aE)^2\right)\Delta_r \right]^{1/2}. \tag{2.25}$$

Moreover, by defining new affine parameter

$$\mathrm{d}\lambda = \frac{\Omega^2}{\Sigma}\mathrm{d}\sigma, \tag{2.26}$$

we can rewrite the four equations related to the motion of null objects above as

$$\frac{dt}{d\lambda} = \frac{\left\{\left(\Delta_r Z_\theta - P\sin^2\theta a Z_r\right) L - \left(\Delta_r Z_\theta^2 - P\sin^2\theta Z_r^2\right) E\right\}}{\sin^2\theta \Delta_r P}, \tag{2.27}$$

$$\frac{\mathrm{d}r}{\mathrm{d}\lambda} = \sqrt{\mathcal{R}}, \tag{2.28}$$

$$\frac{\mathrm{d}\theta}{\mathrm{d}\lambda} = \sqrt{\Theta}, \tag{2.29}$$

and

$$\frac{d\phi}{d\lambda} = \frac{\left\{\left(\Delta_r - P\sin^2\theta a^2\right) L - \left(\Delta_r Z_\theta - P\sin^2\theta a Z_r\right) E\right\}}{\sin^2\theta \Delta_r P}, \tag{2.30}$$

where

$$\Theta = P\left(K + (L - aE)^2\right) - \frac{(L - Z_\theta E)^2}{\sin^2\theta}, \tag{2.31}$$

and

$$\mathcal{R} = (aL - Z_r E)^2 - \left(K + (L - aE)^2\right)\Delta_r. \tag{2.32}$$

The propagation of light in the accelerating KNTN spacetime is determined by Eqs. (2.27)–(2.30). To have a more compact equation, we can introduce the reduced photon constants $\xi = L/E$ and $\eta = K/E^2$. Furthermore, it is understood that Eq. (2.32) can be used to define the shape of the dark zone created by an accelerating black hole with a NUT charge. The boundary of shadow is then given by the following conditions

$$\mathcal{R} = 0 \quad \text{and} \quad \frac{\mathrm{d}\mathcal{R}}{\mathrm{d}r} = 0. \tag{2.33}$$

Accordingly, from the last two equations, we can obtain

$$\xi = \frac{Z_r \Delta_r' - 2\Delta_r Z_r'}{a\Delta_r'}, \tag{2.34}$$

and

$$\eta = -\frac{a^4\left(\Delta_r'\right)^2 + 2\left(2\Delta_r \Delta_r' Z_r' - 2\Delta_r\left(Z_r'\right)^2 - 2Z_r\left(Z_r'\right)^2\right)}{a^2 + \left(2\Delta_r Z_r' - Z_r \Delta_r'\right)^2} \frac{}{a^2\left(\Delta_r'\right)^2}, \tag{2.35}$$

where "prime" denotes the derivative with respect to r.

In Ref. [17], it was shown that the latitudinally stable null circular motion in accelerating black hole spacetime without NUT charge cannot occur on the equatorial plane. One can compute that in the accelerating Kerr spacetime [17]

$$\frac{\mathrm{d}\Theta}{\mathrm{d}\theta} = 2bKm \tag{2.36}$$

at $\theta = \pi/2$ and $L = aE$. This is confirmed by taking the derivative of Θ in Eq. (2.31) with respect to θ for the $n \to 0$ limit. However, for a general NUT charge parameter n, one can show that the condition

$$\alpha_2 b^2 + \alpha_1 b + \alpha_0 = 0 \tag{2.37}$$

where

$$\alpha_2 = a^3 n\eta\left(a^2 + q^2 - n^2\right), \tag{2.38}$$

$$\alpha_1 = -a^2 m\eta\left(a^2 + n^2\right), \tag{2.39}$$

and

$$\alpha_0 = 4n^2\left(a^2 + n^2\right), \tag{2.40}$$

can guarantee

$$\frac{\mathrm{d}\Theta}{\mathrm{d}\theta} = 0 \tag{2.41}$$

for the $L = aE$ case. Therefore, it implies that the existence of NUT and electric charges in the accelerating black hole spacetime can allow the null circular motion provided that the spacetime parameters satisfy Eq. (2.37).

The AKNTN metric encapsulates a rich interplay of gravitational effects. The acceleration parameter, here represented by b, not only introduces the non-trivial conformal factor Ω but also gives rise to additional horizons, i.e. acceleration horizons. These horizons delineate regions where the black hole's acceleration, driven by conical singularities (interpretable as cosmic strings or struts), plays a significant role.

Furthermore, the inclusion of the NUT parameter n introduces a gravitomagnetic charge that twists the spacetime. This twist leads to unusual global properties, such as modified asymptotic behavior and the potential emergence of closed timelike plots, which challenge standard causal structures. The combined effects of rotation (quantified by a), electric charge (q), and the NUT parameter yield a complex horizon structure and significantly influence curvature invariants like the Kretschmann scalar. Notably, while conventional Kerr or Kerr–Newman spacetimes exhibit a point singularity, NUTty spacetimes may replace this with a string-like singularity along the rotational axis.

On the level of geodesic motion, the separability of the Hamilton–Jacobi equation enabled by the ∂_t and ∂_ϕ Killing symmetries allows for a clear analysis of photon trajectories. The introduction of reduced photon constants ξ and η aids in

defining the boundary of the black hole shadow, thereby providing a direct link between the intricate theoretical framework and observable astrophysical phenomena.

3 Black hole shadow

In this work, our investigation of the black hole shadow in AKNTN spacetime adopts the methodology outlined in [35]. However, given that the metric of the accelerating spacetime includes the conformal factor Ω^{-2}, we provide a brief review of the derivation of the impact parameters (x, y) as presented in [35]. This review aims to explore how the results can be adapted to spacetime with a conformal factor, which is the focus of our study. It is important to note that the black hole spacetime discussed in [35] is an asymptotically flat Kerr family.

Similar to the Kerr spacetime, the AKNTN spacetime is also stationary and axially symmetric. Let us now define the observer basis $\{\mathbf{e}_{(t)}, \mathbf{e}_{(r)}, \mathbf{e}_{(\theta)}, \mathbf{e}_{(\phi)}\}$, which can be expanded in the coordinate basis $\{\partial_t, \partial_r, \partial_\theta, \partial_\phi\}$. This expansion is not unique, and one possible choice, as proposed in [35], can be expressed as

$$\begin{aligned} &\mathbf{e}_{(t)} = B^t\partial_t + B^\phi\partial_\phi, \quad \mathbf{e}_{(\phi)} = A^\phi\partial_\phi, \\ &\mathbf{e}_{(\theta)} = A^\theta\partial_\theta, \quad \mathbf{e}_{(r)} = A^r\partial_r, \end{aligned} \tag{3.1}$$

where A^i and B^i for $i = \{t, r, \theta, \phi\}$ are real coefficient functions. The observer basis is normalized as the basis Minkowski spacetime, namely

$$\mathbf{e}_{(i)} \cdot \mathbf{e}_{(j)} = \eta_{(i)(j)}, \tag{3.2}$$

where the non-vanishing components of $\eta_{(i)(j)}$ are

$$\eta_{(r)(r)} = \eta_{(\theta)(\theta)} = \eta_{(\phi)(\phi)} = -\eta_{(t)(t)} = 1. \tag{3.3}$$

It turns out that this set up leads to $A^k = g_{kk}^{-1/2}$ for $k = \{r, \theta, \phi\}$. Another coefficient functions are found to be

$$B^t = \sqrt{\frac{g_{\phi\phi}}{g_{t\phi}^2 - g_{tt}g_{\phi\phi}}} = -\frac{g_{\phi\phi}}{g_{t\phi}}B^\phi. \tag{3.4}$$

By understanding $\mathbf{e}_{(i)} = e^\mu_{(i)}\partial_\mu$, the locally measured momentum $p^{(k)}$ can be obtained by projecting the four-momentum p_μ onto $\mathbf{e}_{(i)}$. The measured energy is given by

$$p^{(t)} = -e^\mu_{(t)}p_\mu = -\left(B^t p_t + B^\phi p_\phi\right). \tag{3.5}$$

Note that the negative sign in the last equations comes from the normalization condition $\mathbf{e}_{(t)} \cdot \mathbf{e}_{(t)} = -1$. Furthermore, recall that $p_t = -E$ and $p_\phi = L$ as the conserved quantities associated with the null test object in spacetime. Therefore, we have

$$p^{(t)} = EB^t - LB^\phi, \tag{3.6}$$

$$p^{(r)} = e^\mu_{(r)}p_\mu = A^r p_r = \frac{p_r}{\sqrt{g_{rr}}}, \tag{3.7}$$

$$p^{(\theta)} = e^\mu_{(\theta)}p_\mu = A^\theta p_\theta = \frac{p_\theta}{\sqrt{g_{\theta\theta}}}, \tag{3.8}$$

and

$$p^{(\phi)} = e^\mu_{(\phi)}p_\mu = A^\phi p_\phi = \frac{L}{\sqrt{g_{\phi\phi}}}. \tag{3.9}$$

As reviewed in [35], the photon's linear momentum $\vec{P}$ is constructed by the components $p^{(r)}$, $p^{(\theta)}$, and $p^{(\phi)}$, i.e.

$$\vec{P}\cdot\vec{P} = \left(p^{(r)}\right)^2 + \left(p^{(\theta)}\right)^2 + \left(p^{(\phi)}\right)^2. \tag{3.10}$$

Accordingly, by using the angular coordinate (α, β), we can have

$$\begin{aligned} p^{(\phi)} &= \left|\vec{P}\right| \sin\beta\cos\alpha \\ p^{(\theta)} &= \left|\vec{P}\right| \sin\alpha \\ p^{(r)} &= \left|\vec{P}\right| \cos\beta\cos\alpha \end{aligned}$$

For the null object like photon, it is understood that $\left|\vec{P}\right|$ is its energy, i.e. $\left|\vec{P}\right| = p^{(t)}$. Using the quantities reviewed above, the shadow's edge of an AKNTN black hole can be expressed analytically.

For our analysis, we adopt a zero angular momentum observer (ZAMO) frame located at (r_o, θ_o). A ZAMO is defined as an observer whose angular momentum, as measured at infinity, vanishes. This choice is particularly advantageous in rotating spacetimes, as it minimizes the direct influence of frame-dragging on the locally measured photon momenta. In effect, the ZAMO frame provides a clear and intuitive basis for mapping the incoming photon directions to impact parameters on the observer's celestial sphere, thereby simplifying the interpretation of the black hole shadow.

The choice of a ZAMO frame is particularly useful because it establishes a locally non-rotating reference in which the observer's measurements of the photon momentum are more directly related to the geometry of the black hole shadow. In this frame, an observer facing the black hole naturally has a radial momentum component satisfying $p^{(r)} \geq 0$. Consequently, the locally measured momentum components can be mapped onto angular coordinates α and β on the observer's celestial sphere via

$$\alpha = \sin^{-1}\left(\frac{p^{(\theta)}}{p^{(t)}}\right), \quad \beta = \tan^{-1}\left(\frac{p^{(\phi)}}{p^{(r)}}\right). \tag{3.11}$$

This mapping directly translates the local measurements in the ZAMO frame to the impact parameters that define the black hole shadow. In other words, by ensuring that the observer is non-rotating (i.e. having zero angular momentum), the measured components $p^{(r)}$, $p^{(\theta)}$, and $p^{(\phi)}$ can be unambiguously related to the angles α and β, which in turn determine the observed silhouette of the black hole.

Hence, the exact closed form of these angular coordinates (α, β) related to the AKNTN black hole (2.1) can be expressed as

$$\sin\alpha = \pm \left.\frac{(Z_r - aZ_\theta)}{(Z_r - a\xi_p)\sin^2\theta Z_r \Sigma}\sqrt{H}\right|_{r=r_o,\theta=\theta_o}, \tag{3.12}$$

and

$$\tan\beta = \left.\frac{\xi_p \Sigma\sqrt{\Delta_r}}{\sqrt{\left((a^2-\Delta_r)\xi_p{}^2 + 2a(\Delta_r - Z_r)\xi_p - \left(a^2+\eta_p\right)\Delta_r + Z_r\right)\left(PZ_r^2\sin^2\theta - \Delta_r Z_\theta{}^2\right)}}\right|_{r=r_o,\theta=\theta_o}, \tag{3.13}$$

where

$$H = \Delta_r\left(\Delta_r Z_\theta{}^2 - PZ_r^2\sin^2\theta\right) \times\left[\left(\xi_p - Z_\theta\right)^2 - \left(\left(\xi_p - a\right)^2 + \eta_p\right)P\sin^2\theta\right]. \tag{3.14}$$

In equations above, $\xi_p = \xi\left(r = r_p\right)$ and $\eta_p = \eta\left(r = r_p\right)$, namely the reduced photon constants ξ and η that correspond to the photon sphere near AKNTN black hole. At equator, $\theta = \pi/2$, these angular coordinates can be expressed as

$$\sin\alpha_{\text{eq.}} = \pm\frac{\left(Z_r - a^2 - 2na\right)}{\left(Z_r - a\xi\right)Z_r^2}\sqrt{H_{\text{eq.}}}, \tag{3.15}$$

and

$$\tan\beta_{\text{eq.}} = \frac{\xi\Sigma\sqrt{\Delta_r}}{\sqrt{\left((a^2-\Delta_r)\xi^2 + 2a(\Delta_r - Z_r)\xi - \left(a^2+\eta\right)\Delta_r + Z_r\right)\left(P_{\text{eq.}}Z_r^2 - \Delta_r(a+2n)\right)}}, \tag{3.16}$$

where

$$P_{\text{eq.}} = \left(1 - \frac{bar_+(a+n)}{a^2+n^2}\right)\left(1 - \frac{bar_-(a+n)}{a^2+n^2}\right), \tag{3.17}$$

and

$$H_{\text{eq.}} = \Delta_r\left(\Delta_r(a+2n)^2 - P_{\text{eq.}}Z_r^2\right) \times\left[(\xi - a - 2n)^2 - \left((\xi-a)^2 + \eta\right)P_{\text{eq.}}\right]. \tag{3.18}$$

Based on the angular coordinates (α, β) and the observer's location, we can define the Cartesian coordinate

$$x = -r_o\cos\alpha\sin\beta \ , \quad y = r_o\sin\alpha, \tag{3.19}$$

to map the shadow of an observed black hole.

To illustrate the shadow of AKNTN black hole based on the results above, below we provide some numerical evaluations of the shadow by varying some incorporated parameters. In producing the numerical plots, we consider $r_o = 30\,m$. Figure 2 depict the shadow's profile for two rotational parameters, $a^* = 0.9$ and $a^* = 0.999$, at $\theta_o = \pi/2$, while varying the acceleration parameter b^*. The cases $b^* = 0$, $b^* = 0.01$, and $b^* = 0.02$ are represented by black, blue, and red plots, respectively.[1] As the acceleration parameter increases, the shadow's edge shrinks, indicating a reduction in the photon capture region. This behavior aligns with the theoretical predictions outlined in [17]. The shrinking of the shadow can be attributed to the altered geometry induced by the acceleration, which affects the critical photon orbits around the black hole. Furthermore, increasing the rotational parameter a^* leads to the flattening on the shadow's left side. This characteristic arises from the frame-dragging effect, which becomes more pronounced for higher rotation rates. Such flattening reflects the asymmetry introduced by the black hole's angular momentum, an effect well-documented in Kerr-like spacetimes [12,35].

On the other hand, the variation of the black hole shadow as the observer's latitude coordinate changes is presented in Fig. 3. The plots are labeled using three different line styles to represent distinct values of $\sin\theta_o$, i.e. the dotted lines correspond to $\sin\theta_o = 1$, the dashed lines to $\sin\theta_o = 0.8$, and the dashed-dotted lines to $\sin\theta_o = 0.6$. Figure 3a illustrates the non-accelerating case ($b^* = 0$), while Fig. 3b depicts the scenario with acceleration ($b^* = 0.02$). In both figures, the NUT parameter is assumed to vanish. While the general profile of the shadow remains similar across these cases, the introduction of acceleration reduces the shadow's

[1] In this paper we use the "starred" notation to denote the dimensionless parameters.

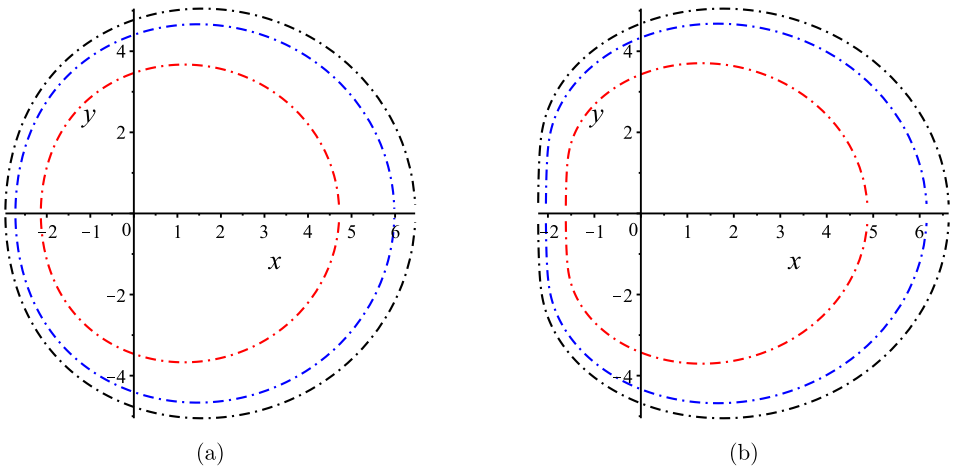

Fig. 2 Shadow of AKNTN black hole for an observer at $\theta_o = \pi/2$ and $r_o^* = 30$ for several acceleration parameters. The increasing acceleration parameter yields to the shrinking of the shadow's edge, as pointed in [17]. Here we consider $q^* = 0.1$, $n^* = 0.1$. The black, blue, and red plots represent the $b^* = 0$, $b^* = 0.01$, and $b^* = 0.02$ cases, respectively. The case $a^* = 0.9$ is described by **a**, whereas the $a^* = 0.999$ is depicted by **b**. As usual, the "left" side of the shadow gets flattened as the rotational parameter increases

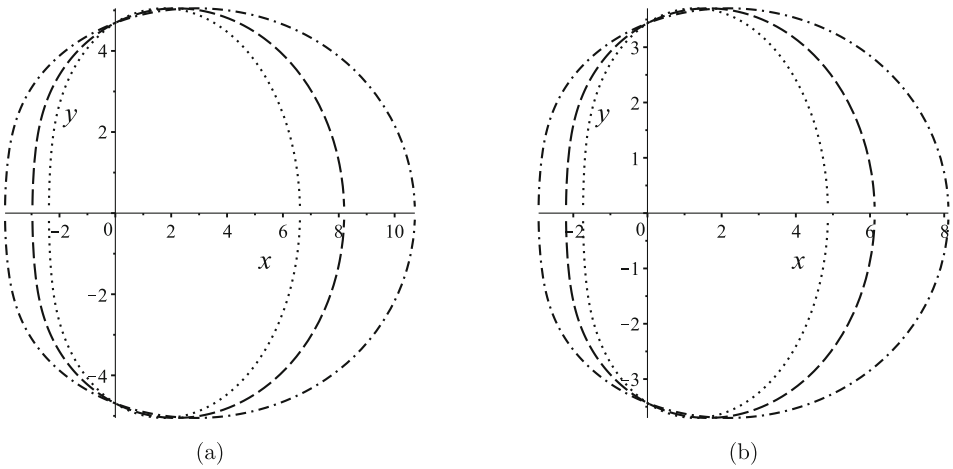

Fig. 3 The dots, dashed, and dashed-dots plots represent the cases of $\sin\theta_o = 1$, $\sin\theta_o = 0.8$, and $\sin\theta_o = 0.6$. The $b^* = 0$ case is represented by **a**, whereas **b** describes the case with acceleration, namely $b^* = 0.02$. Here we consider $q^* = 0.1$, $a^* = 0.99$, $n^* = 0.1$, and $r_o^* = 30$. Note that the general profile of the two figures are similar, only the size of the shadow area gets smaller for the accelerating case

overall size, as evident when comparing the two figures. This highlights the impact of the acceleration parameter on the observable shadow of the black hole.

To offer a clear comparison of the black hole shadows within the AKNTN family, Fig. 4 present representative numerical examples that illustrate the influence of the additional parameters q (electric charge), n (NUT parameter), and b (acceleration) on the shadow. Specifically, Fig. 4a displays the shadows, as seen by an equatorial observer ($\theta_0 = \pi/2$), for four distinct non-accelerating cases: Kerr, Kerr–Newman, Kerr–Taub–NUT, and Kerr–Newman–Taub–NUT. In contrast, Fig. 4b shows the corresponding accelerating solutions. In all plots, the dimensionless parameters are fixed at $b^* = 0.02$, $q^* = 0.4$, $a^* = 0.09$, and $n^* = 0.1$.

Figure 4a demonstrates that adding an electric charge (q^*) reduces the overall shadow size compared to the uncharged Kerr solution. Conversely, the inclusion of a NUT parameter (n^*) enlarges the effective shadow size, consistent with the findings in [36]. Moreover, a direct comparison with Fig. 4b reveals that the introduction of acceleration further compresses the photon capture region, resulting in a smaller shadow radius. Such behavior is also reported in [17]. Notably, the previously observed effect of the NUT parameter in enlarging the shadow persists even in the presence of acceleration.

4 Tidal charge and the black hole shadow

In the RS-II braneworld scenario [37], the dynamics of gravity in our four-dimensional universe (the brane) are influenced by the higher-dimensional bulk. By projecting the five-dimensional Einstein equations,

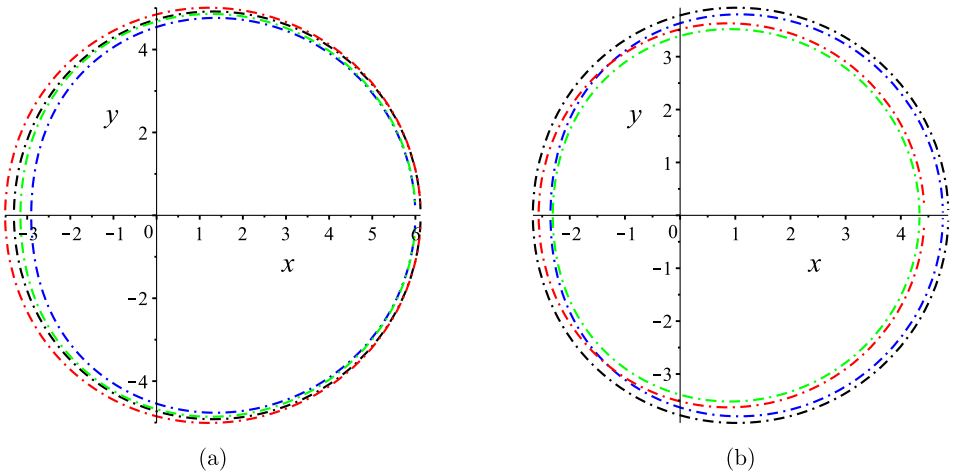

Fig. 4 In **a**, the shadow edges observed by an observer at equator and $r_o^* = 30$ for the Kerr, Kerr–Newman, Kerr–Taub–NUT, and Kerr–Newman–Taub–NUT black holes are shown by the black, blue, red, and green plots, respectively. The corresponding accelerating cases for each of these configurations are presented in **b**. The physical parameters used in generating these plots are $b^* = 0.02$, $q^* = 0.4$, $a^* = 0.09$, and $n^* = 0.1$

$$^{(5)}G_{MN} + \Lambda_5 \bar{g}_{MN} = \kappa_5^2 T_{MN}, \tag{4.1}$$

onto the brane using the Gauss–Codazzi formalism and imposing $\mathbb{Z}_2$ symmetry, one obtains effective four-dimensional gravitational field equations. These take the form [31,38]

$$G_{\mu\nu} + \Lambda_4\, g_{\mu\nu} + E_{\mu\nu} = 0, \tag{4.2}$$

where $E_{\mu\nu}$ is the projection of the five-dimensional Weyl tensor onto the brane:

$$E_{\mu\nu} = {}^{(5)}C_{KLMN}\, n^K n^M e^L_\mu e^N_\nu. \tag{4.3}$$

In the absence of a brane cosmological constant (i.e. $\Lambda_4 = 0$), this reduces to

$$G_{\mu\nu} = -E_{\mu\nu}. \tag{4.4}$$

The term $E_{\mu\nu}$ encapsulates the nonlocal gravitational effects from the bulk and can be interpreted as contributing a "tidal charge" to the effective four-dimensional metric. In practice, this tidal charge is introduced by replacing the electric charge term q^2 in the standard AKNTN metric with a tidal parameter $\mathcal{Q}$, which may take either positive or negative values, thereby modifying the horizon structure and influencing observable quantities such as the black hole shadow. As discussed in [31, 39–41], the traceless tensor $E_{\mu\nu}$ is assumed to exist to satisfy the corresponding Einstein equations. This tensor originates from bulk geometrical effects, and to date, the exact bulk spacetime geometry that yields the precise brane spacetime described in [31,39–41] remains unknown.

Here, we construct the accelerating, tidal charged, and rotating Taub–NUT black hole solution within the RS-II braneworld scenario, following the approach presented in Refs. [29–32]. We assume the existence of the corresponding $E_{\mu\nu}$ and determine the spacetime metric components using the trace of the effective Einstein equation. The AKNTN black hole solution in Eq. (2.1) can also be used to represent a tidal charged and electrically neutral accelerating Taub–NUT black hole within the RSII framework, with the condition that q^2 is replaced by the tidal parameter $\mathcal{Q}$, where $\mathcal{Q}$ can take both positive and negative values. To express the metric solution for the tidal charged accelerating and rotating Taub–NUT black hole in the RSII model, we simply consider the metric (2.1) with

$$r_\pm = m \pm \sqrt{m^2 + n^2 - a^2 - \mathcal{Q}}, \tag{4.5}$$

where the corresponding components of $E_{\mu\nu}$ tensor are given in the appendix. Obviously, the condition $m^2+n^2-a^2-\mathcal{Q} \geq 0$ must hold for black hole spacetime.

The possibility for a negative $\mathcal{Q}$ will contribute uniquely to the shape of the black hole shadow, distinguishing it from the typical accelerating electrically charged black hole discussed in the previous section. In Fig. 5, the cases of positive and negative tidal charge are represented by the dots and dashed-dotted plots, respectively. A noticeable feature distinguishing the two is the shadow area, where the area corresponding to negative $\mathcal{Q}$ is larger than that for the positive value. A negative tidal charge, $\mathcal{Q} < 0$, effectively deepens the gravitational potential, thereby enlarging the photon capture region and resulting in a larger shadow. In contrast, a positive tidal charge, $\mathcal{Q} > 0$, reduces the gravitational pull, leading to a smaller shadow.

5 Observables

The black hole shadow presented in the previous section can vary as the incorporated parameters change. Nevertheless, it is not easy to discern how one shadow differs from another. Therefore, it is useful to introduce certain quantities that serve as observables for the shadow. Examples of such observables are the shadow radius R_s and the distortion parameter δ_s introduced in [34]. The shadow radius R_s is a measure of the

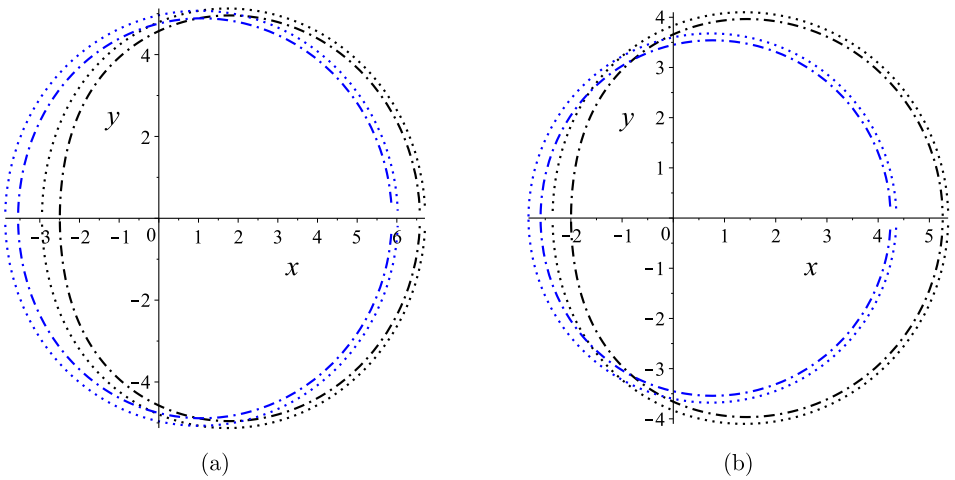

Fig. 5 Plots above are evaluated for $a^* = 0.9$ and for equatorial observers at $r_o^* = 30$. **a** For vanishing acceleration parameter, whereas **b** For $b^* = 0.02$. The dots plot for $\mathcal{Q}^* = -0.1$, and dashed-dots one represents the $\mathcal{Q}^* = 0.1$ case. Black plots describe the vanishing NUT parameter, whereas the blue ones correspond to the $n^* = 0.1$ consideration

overall size of the shadow, whereas the distortion δ_s quantifies deviations from circularity.

The shadow radius represents the radius of an imaginary reference circle that best approximates the shadow's contour, while the distortion parameter quantifies the deviation of the actual shadow contour from this reference circle. These observables have also been evaluated for black hole shadows in various spacetimes, including the Kerr–Taub–NUT spacetime [36], the NUT spacetime with the Manko-Ruiz parameter [42], and accelerating black hole spacetimes [17]. These observables are defined as

$$R_s = \frac{(X_R - X_M)^2 + Y_M^2}{2\,(X_R - X_M)}, \tag{5.1}$$

and

$$\delta_s = \frac{X_L - X_R + 2R_s}{R_s}, \tag{5.2}$$

where the schematic of the associated points is illustrated in Fig. 6.

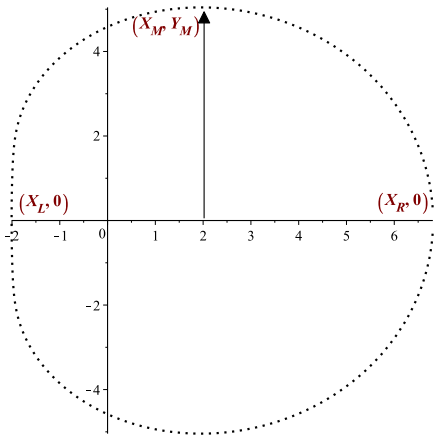

Fig. 6 Schematic of the black hole shadow showing the points required to compute the shadow observables R_s and δ_s in Eqs. (5.1) and (5.2). Here, X_L and X_R denote the leftmost and rightmost points of the shadow edge, while (X_M, Y_M) is the topmost point

We numerically investigate the shadow observables of the accelerating Kerr–Newman–Taub–NUT black hole with respect to several key parameters, including the acceleration parameter b, the electric charge q, the spin a, and the NUT parameter n. The effects of the black hole charge q (or, equivalently, the tidal charge $\mathcal{Q}$) on the shadow observables are illustrated in Fig. 7. First, we consider the case of the accelerating Kerr–Newman–Taub–NUT black hole (AKNTN) within the framework of Einstein–Maxwell theory, where $q^2 \geq 0$. In this scenario, both the normalized shadow radius R_s^* and the distortion parameter δ_s decrease as the charge q increases. In contrast, for a negative tidal charge $\mathcal{Q}$, the results in Fig. 7 reveal that both the shadow radius and the distortion parameter increase as the absolute value of $\mathcal{Q}$ grows. Furthermore, the shadow radius R_s^* decreases as the acceleration parameter b^* increases, indicating that acceleration consistently reduces the shadow size.

Figures 8 and 9 provide further insights into the dependence of the shadow observables on the spin a and the acceleration parameter b^*. In Fig. 8a, the shadow radius R_s is shown to increase with increasing spin a. The plots corresponding to $b^* = 0$, $b^* = 0.01$, and $b^* = 0.02$ are represented by dots, dashed, and dash-dotted plots, respectively. As observed earlier, the shadow radius R_s decreases as the acceleration parameter b^* increases. The distortion parameter δ_s, depicted in Fig. 8b, is analyzed for both accelerating and non-accelerating cases, further illustrating the influence of spin and acceleration on the shadow geometry. The impact of the acceleration parameter b^* on the shadow observables is explored in greater detail in Fig. 9. In Fig. 9a, the shadow radius R_s is presented, and in Fig. 9b, the distortion parameter δ_s is shown for different values of the normalized NUT parameter n^*; specifically, $n^* = 0$, $n^* = 0.1$, and $n^* = 0.2$ are represented by dots, dashed, and dash-dotted plots, respectively. The results in Figs. 7, 8, and 9 demonstrate that both R_s and δ_s significantly depend on b^*, n^*, q,

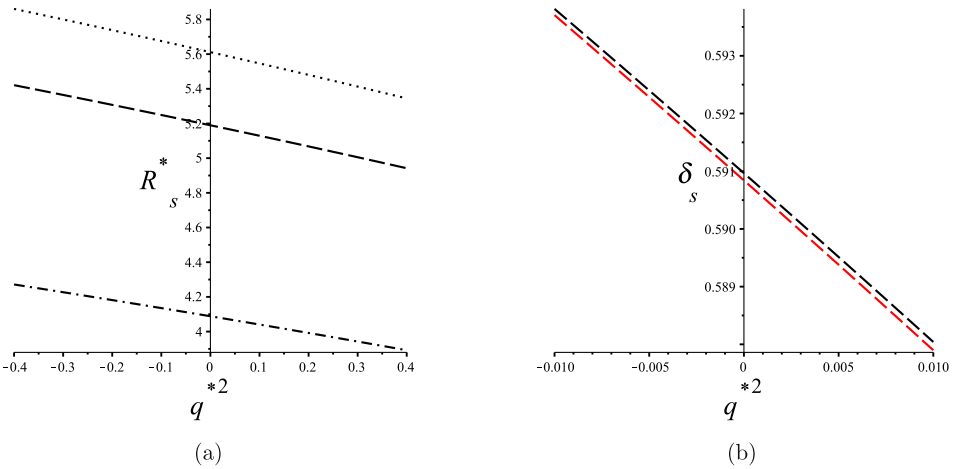

(a) (b)

Fig. 7 In **a**, the dots, dashed, and dash-dotted plots represent the cases of $b^* = 0$, $b^* = 0.01$, and $b^* = 0.02$, respectively. In **b**, the red plot corresponds to the non-accelerating case, whereas the black plot represents the $b^* = 0.02$ case. Here, we have considered $a^* = 0.9$, $n^* = 0.1$, $\theta_o = \pi/2$, and $r_o^* = 30$. In these figures, we consider negative values for q^{*2} to model the negative tidal charge $\mathcal{Q}$ associated with the braneworld black hole discussed earlier. Recall that the electric charge q in the Kerr–Newman solution is related to the tidal charge by $\mathcal{Q} = q^2$

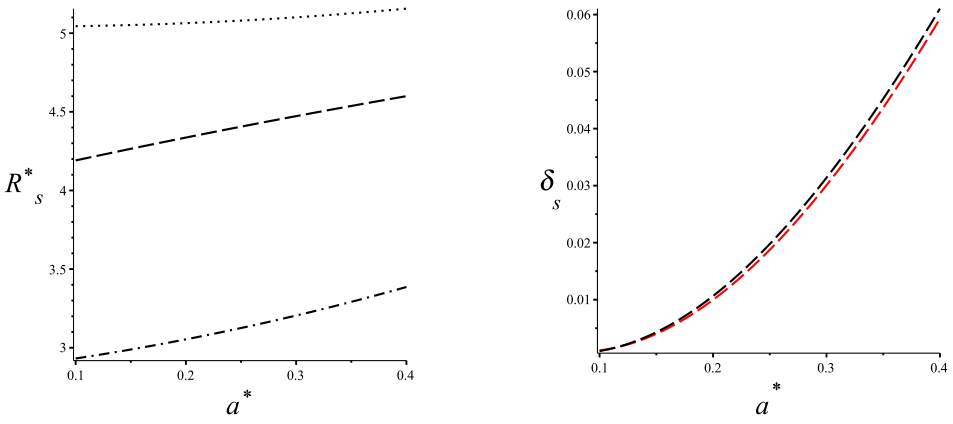

(a) (b)

Fig. 8 In **a**, the dots, dashed, and dash-dotted plots represent the cases of $b^* = 0$, $b^* = 0.01$, and $b^* = 0.02$, respectively. In **b**, the red plot corresponds to the non-accelerating case, whereas the black plot represents the $b^* = 0.02$ case. Here, we have considered $q^* = 0.1$, $n^* = 0.1$, $\theta_o = \pi/2$, and $r_o^* = 30$

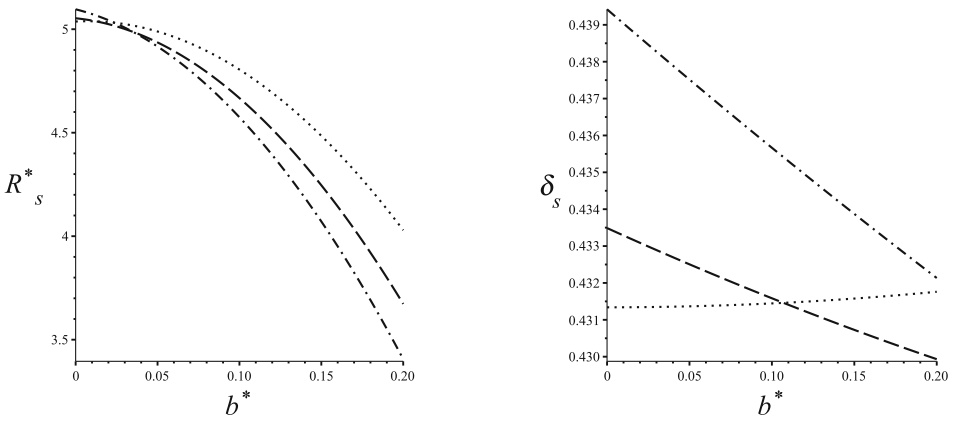

(a) (b)

Fig. 9 In **a** and **b**, the dots, dashed, and dash-dotted plots represent the cases of $n^* = 0$, $n^* = 0.1$, and $n^* = 0.2$, respectively. Here, we have considered $a^* = 0.9$, $q^* = 0.1$, $\theta_o = \pi/2$, and $r_o^* = 30$

and a, underscoring the complex interplay between the NUT parameter, acceleration, charge, and spin in determining the characteristics of the black hole shadow.

We now take a closer look at the results depicted in Fig. 9a. We observe that R_s decreases as b grows. Such behavior is also reported in [17]. It can be understood that increasing the acceleration parameter modifies the spacetime geometry via the conformal factor, which effectively "compresses" the region where unstable photon orbits (i.e., the photon sphere) exist. This compression reduces the effective size of the photon capture region, leading to a smaller shadow radius R_s. In other words, a higher acceleration alters the gravitational field in such a way that photons can only be captured at smaller radii, thus producing a diminished shadow when observed at infinity.

Furthermore, as shown in Refs. [36,42], the shadow size in NUTty spacetimes generally increases with the NUT parameter. This behavior is indeed observed in Fig. 9a for small values of the acceleration parameter, including the non-accelerating case. However, an opposite trend emerges for larger values of b. Specifically, in accelerating black hole spacetimes with significant acceleration, the shadow radius R_s decreases as the NUT parameter increases. This reversal in the dependence of R_s on the NUT parameter is a distinctive feature of accelerating NUT spacetimes, highlighting the intricate interplay between acceleration and the NUT parameter.

Before concluding, we briefly discuss how the shadow analysis of the AKNTN black hole, as presented in this paper, relates to astrophysical observations by the Event Horizon Telescope (EHT) [43,44]. The modifications introduced by the accelerating Kerr–Newman–Taub–NUT (AKNTN) metric have potential observational consequences for black hole shadow studies, particularly with instruments such as the Event Horizon Telescope (EHT). Our analysis reveals that the inclusion of an acceleration parameter compresses the photon capture region, leading to a smaller shadow radius relative to the standard Kerr prediction. Additionally, the presence of a NUT parameter introduces asymmetries and shape distortions not present in a pure Kerr geometry.

Although current EHT observations of M87* [43] and Sgr A* [44] are largely consistent with the Kerr hypothesis, the deviations predicted by the AKNTN model, such as the reduced shadow size due to acceleration and the enhanced distortions from the NUT charge, could become detectable with future improvements in observational resolution. In the context of the RS-II braneworld scenario, a negative tidal charge ($\mathcal{Q} < 0$) further deepens the gravitational potential and enlarges the shadow, offering another potential observational signature.

6 Conclusion and discussion

In this work, we have explored the black hole shadow in the accelerating Kerr–Newman–Taub–NUT (AKNTN) spacetime, thereby extending previous investigations of NUTty spacetimes [36,42] and accelerating black holes [17]. The exact AKNTN solution [6–8] enabled us to derive a separable Hamilton–Jacobi equation for null geodesics, revealing that the additional parameters allow for equatorial circular photon orbits-an effect absent in generic accelerating spacetimes. We also demonstrated that the AKNTN metric can be interpreted within the RS-II braneworld scenario, with effective tidal charges emerging from bulk effects.

Our numerical analysis shows that the shadow's size and shape are strongly influenced by the acceleration, spin, electric (or tidal) charge, and NUT parameter. In particular, increasing the acceleration compresses the photon capture region, thereby reducing the shadow radius R_s. For electrically charged black holes, a higher charge diminishes the shadow size, whereas a negative tidal charge ($\mathcal{Q} < 0$) deepens the gravitational potential and enlarges the shadow. Moreover, the NUT parameter exhibits a nontrivial influence: for small values the shadow grows with the NUT charge, but for larger values, the trend reverses.

These results not only deepen our understanding of the intricate interplay between the spacetime parameters and observable shadow features but also provide a potential pathway for confronting theoretical predictions with astrophysical observations. Future work may explore the thermodynamic properties, Hawking radiation, and stability under perturbations of AKNTN black holes, as well as their extensions to modified gravity theories and higher-dimensional scenarios. Such investigations promise to further illuminate the rich physics underlying these exotic spacetimes.

Acknowledgements This work was supported by LPPM-UNPAR through the Penelitian Publikasi Internasional Bereputasi funding scheme. We gratefully acknowledge the anonymous reviewer for his/her comments and suggestions, which have improved the clarity of this manuscript.

Data Availability Statement Data will be made available on reasonable request. [The datasets generated during and/or analysed during the current study are available from the corresponding author on reasonable request.].

Code Availability Statement Code/software will be made available on reasonable request. [The code/software generated during and/or analysed during the current study is available from the corresponding author on reasonable request.].

Funded by SCOAP[3].

A Components of $E_{\mu\nu}$ for a tidal charged and electrically neutral accelerating NUT black hole

The components of $E_{\mu\nu}$ as the bulk effect on the brane are

$$
\begin{aligned}
E_{tt} = & \frac{\left(a^2 br\cos\theta + barn - a^2 - n^2\right)^2 \mathcal{Q}}{\left(a^2+n^2\right)^4 \Sigma^3} \\
& \times \Big\{ a^6 b^2 \left(a^2 - n^2 + \mathcal{Q}\right)\cos^4\theta \\
& +2a^4 b\left(na^3 b - n^3 ab + \mathcal{Q} abn - ma^2 - n^2 m\right)\cos^3\theta \\
& -2a^4 b\left(na^3 b - n^3 ab + \mathcal{Q} abn - ma^2 - n^2 m\right)\cos\theta \\
& -a^2\Big(a^6 b^2 - 2a^4 b^2 n^2 + a^2 b^2 n^4 + a^4 b^2 \mathcal{Q} - a^2 n^2 b^2 \mathcal{Q} \\
& +2na^3 bm + 2n^3 abm - a^4 - 2a^2 n^2 - n^4\Big)\cos^2\theta \\
& -a^6 b^2 n^2 + a^6 b^2 r^2 + a^4 b^2 n^4 \\
& -2a^4 b^2 n^2 r^2 - 2a^4 b^2 mr^3 + a^4 b^2 r^4 \\
& +a^2 b^2 n^4 r^2 + 2a^2 b^2 n^2 mr^3 \\
& -a^2 b^2 n^2 r^4 - a^4 b^2 n^2 \mathcal{Q} + a^4 b^2 \mathcal{Q} r^2 - a^2 b^2 n^2 \mathcal{Q} r^2 \\
& +2a^5 bnm + 2a^5 bnr + 2a^3 bn^3 m - 4a^3 bnmr^2 \\
& +2a^3 bnr^3 - 2abn^5 r - 4abn^3 mr^2 + 2abn^3 r^3 \\
& +2a^3 bn\mathcal{Q} r + 2abn^3 \mathcal{Q} r - 2a^6 - 3a^4 n^2 \\
& +2a^4 mr - a^4 r^2 + 4a^2 n^2 mr - 2a^2 n^2 r^2 + n^6 \\
& +2n^4 mr - n^4 r^2 - a^4 \mathcal{Q} - 2a^2 n^2 \mathcal{Q} - n^4 \mathcal{Q}\Big\}, \qquad \text{(A.1)}
\end{aligned}
$$

$$
\begin{aligned}
E_{t\phi} = & \frac{\left(a^2 br\cos\theta + barn - a^2 - n^2\right)^2 \mathcal{Q}(1-\cos\theta)}{} \\
& \times\left(a^2+n^2\right)^4 \Sigma^3 \Big\{ a^5 b^2 \left(a^2 + 2na + n^2 + r^2\right) \\
& \times \left(a^2 - n^2 + \mathcal{Q}\right)\cos^3\theta \\
& + \left(a^2 + 2na + n^2 + r^2\right) ba^3 \left(a^4 b + 2na^3 b - a^2 n^2 b\right. \\
& \left. -2n^3 ab + \mathcal{Q} a^2 b + 2\mathcal{Q} abn - 2ma^2 - 2n^2 m\right)\cos^2\theta \\
& +a\Big(2nb^2 a^7 + 5a^6 b^2 n^2 - a^6 b^2 r^2 + 2n^3 b^2 a^5 \\
& +2a^5 b^2 nr^2 - 4a^4 b^2 n^4 + 3a^4 b^2 n^2 r^2 \\
& +2a^4 b^2 mr^3 - a^4 b^2 r^4 \\
& -4n^5 b^2 a^3 - 2a^3 b^2 n^3 r^2 - n^6 b^2 a^2 \\
& -2a^2 b^2 n^4 r^2 - 2a^2 b^2 n^2 mr^3 + a^2 b^2 n^2 r^4 \\
& +2a^5 b^2 n\mathcal{Q} + 5a^4 b^2 n^2 \mathcal{Q} \\
& -a^4 b^2 \mathcal{Q} r^2 + 4\mathcal{Q} a^3 b^2 n^3 + 2\mathcal{Q} a^3 b^2 nr^2 \\
& +\mathcal{Q} a^2 b^2 n^4 + 2a^2 b^2 n^2 \mathcal{Q} r^2 - 2a^6 bm \\
& -6a^5 bnm - 2a^5 bnr - 8a^4 bn^2 m \\
& -2a^4 bmr^2 - 8a^3 bn^3 m + 2a^3 bnmr^2 - 2a^3 bnr^3 \\
& -6a^2 bn^4 m - 2a^2 bn^2 mr^2 - 2abn^5 m \\
& +2abn^5 r + 2abn^3 mr^2 \\
& -2abn^3 r^3 - 2a^3 bn\mathcal{Q} r - 2abn^3 \mathcal{Q} r + 2a^6 + 2a^5 n \\
& +4a^4 n^2 - 2a^4 mr + 2a^4 r^2 + 4a^3 n^3 + 2a^2 n^4 \\
& -4a^2 n^2 mr + 4a^2 n^2 r^2 \\
& +2an^5 - 2n^4 mr + 2n^4 r^2 + a^4 \mathcal{Q} + 2a^2 n^2 \mathcal{Q} + n^4 \mathcal{Q}\Big) \\
& \cos\theta a^7 b^2 n^2 - a^7 b^2 r^2 + 2a^6 b^2 n^3 \\
& -2a^6 b^2 nr^2 + 3a^5 b^2 n^2 r^2 \\
& +2a^5 b^2 mr^3 - a^5 b^2 r^4 - 2a^4 b^2 n^5 \\
& +4a^4 b^2 n^3 r^2 + 4a^4 b^2 nmr^3 - 2a^4 b^2 nr^4 \\
& -a^3 b^2 n^6 - 2a^3 b^2 n^4 r^2 \\
& -2a^3 b^2 n^2 mr^3 + a^3 b^2 n^2 r^4 - 2a^2 b^2 n^5 r^2 \\
& -4a^2 b^2 n^3 mr^3 + 2a^2 b^2 n^3 r^4 + a^5 b^2 n^2 \mathcal{Q} \\
& -a^5 b^2 \mathcal{Q} r^2 + 2a^4 b^2 n^3 \mathcal{Q} \\
& -2a^4 b^2 n\mathcal{Q} r^2 + a^3 b^2 n^4 \mathcal{Q} + 2a^3 b^2 n^2 \mathcal{Q} r^2 \\
& +2a^2 b^2 n^3 \mathcal{Q} r^2 - 2a^6 bnm + 8a^3 bn^2 mr^2 \\
& -4a^3 bn^2 r^3 - 2a^2 bn^5 m \\
& +2a^2 bn^5 r - 2a^6 bnr - 4a^5 bn^2 m - 4a^5 bn^2 r \\
& -4a^4 bn^3 m + 2a^4 bnmr^2 - 2a^4 bnr^3 - 4a^3 bn^4 m \\
& +2a^2 bn^3 mr^2 - 2a^2 bn^3 r^3 + 4abn^6 r \\
& +8abn^4 mr^2 - 4abn^4 r^3 - 2a^4 bn\mathcal{Q} r - 4a^3 bn^2 \mathcal{Q} r \\
& -2a^2 bn^3 \mathcal{Q} r \\
& +4a^6 l + 4a^5 n^2 - 2a^5 mr + 2a^5 r^2 + 6a^4 n^3 \\
& -4a^4 nmr + 2a^4 nr^2 + 2a^3 n^4 - 4a^3 n^2 mr \\
& +4a^3 n^2 r^2 - 8a^2 n^3 mr \\
& +4a^2 n^3 r^2 - 2an^4 mr + 2an^4 r^2 \\
& -4abn^4 \mathcal{Q} r + 2a^7 \\
& -2n^7 - 4n^5 mr + 2n^5 r^2 + a^5 \mathcal{Q} + 2a^4 nQ \\
& +2a^3 n^2 \mathcal{Q} + 4a^2 n^3 \mathcal{Q} + an^4 Q \\
& +2n^5 \mathcal{Q}\Big\}, \qquad \text{(A.2)}
\end{aligned}
$$

$$
E_{rr} = -\frac{\left(a^2 br\cos\theta + barn - a^2 - n^2\right)^2 \mathcal{Q}}{\left(ba^2 r + barn - a^2 - n^2\right)\left(ba^2 r - barn + a^2 + n^2\right)}, \qquad \text{(A.3)}
$$

$$
\begin{aligned}
E_{\theta\theta} = & -\frac{\left(a^2 br\cos\theta + barn - a^2 - n^2\right)^2 \mathcal{Q}}{\Sigma\,(r-r_+)\,(r-r_-)} \\
& \times \frac{1}{\left(2abm\,(n + a\cos\theta) - (n + a\cos\theta)\,abr_+ - a^2 - n^2\right)}, \qquad \text{(A.4)}
\end{aligned}
$$

and

$$
E_{\phi\phi} = -\frac{\left(a^2 br\cos\theta + barn - a^2 - n^2\right)^2 \mathcal{Q}(1-\cos\theta)}{\Sigma^3\left(a^2+n^2\right)^4} \sum_{k=0}^{3} f_k \cos^k\theta, \qquad \text{(A.5)}
$$

where

$$
\begin{aligned}
f_3 = a^2 \Big(& b^2a^8 + 4b^2na^7 + 5a^6b^2n^2 + 3a^6b^2r^2 \\
& + 4a^5b^2nr^2 - 2a^4b^2mr^3 - 5a^4b^2n^4 - 2a^4b^2n^2r^2 \\
& + 2a^4b^2r^4 - 4a^3b^2n^5 - 4a^3b^2n^3r^2 + 2a^2b^2mn^2r^3 \\
& - a^2b^2n^6 - a^2b^2n^4r^2 - 2a^2b^2n^2r^4 + a^6b^2\mathcal{Q} \\
& + 4\mathcal{Q}a^5b^2n + 6\mathcal{Q}a^4b^2n^2 + 3a^4b^2\mathcal{Q}r^2 + 4\mathcal{Q}a^3b^2n^3 \\
& + 4\mathcal{Q}a^3b^2nr^2 + \mathcal{Q}a^2b^2n^4 + \mathcal{Q}a^2b^2n^2r^2 \\
& + \mathcal{Q}a^2b^2r^4 + 2a^5bnr - 4a^3bmnr^2 + 2a^3bnr^3 \\
& - 4abmn^3r^2 - 2abn^5r + 2abn^3r^3 + 2\mathcal{Q}a^3bnr \\
& + 2\mathcal{Q}abn^3r - a^6 + 2a^4mr - a^4n^2 - a^4r^2 \\
& + 4a^2mn^2r + a^2n^4 - 2a^2n^2r^2 + 2mn^4r + n^6 \\
& - n^4r^2 - a^4\mathcal{Q} - 2\mathcal{Q}a^2n^2 - \mathcal{Q}n^4 \Big),
\end{aligned} \tag{A.6}
$$

$$
\begin{aligned}
f_2 = a \Big(& b^2a^9 + 6b^2na^8 + 13a^7b^2n^2 + 3a^7b^2r^2 \\
& + 10a^6b^2n^3 + 12a^6b^2nr^2 - 2a^5b^2mr^3 \\
& - 5a^5b^2n^4 + 6a^5b^2n^2r^2 + 2a^5b^2r^4 - 8a^4b^2mnr^3 \\
& - 14a^4b^2n^5 - 12a^4b^2n^3r^2 + 6a^4b^2nr^4 + 2a^3b^2mn^2r^3 \\
& - 9a^3b^2n^6 - 9a^3b^2n^4r^2 - 2a^3b^2n^2r^4 + 8a^2b^2mn^3r^3 \\
& - 2a^2b^2n^7 - 6a^2b^2n^3r^4 + \mathcal{Q}a^7b^2 + 6\mathcal{Q}a^6b^2n \\
& + 14\mathcal{Q}a^5b^2n^2 + 3a^5b^2\mathcal{Q}r^2 + 16\mathcal{Q}a^4b^2n^3 \\
& + 12\mathcal{Q}a^4b^2nr^2 + 9\mathcal{Q}a^3b^2n^4 + 9\mathcal{Q}a^3b^2n^2r^2 + \mathcal{Q}a^3b^2r^4 \\
& + 2\mathcal{Q}a^2b^2n^5 + 2\mathcal{Q}a^2b^2nr^4 - 2a^7bm - 8a^6bmn \\
& + 2a^6bnr - 14a^5bmn^2 - 4a^5bmr^2 + 8a^5bn^2r \\
& - 16a^4bmn^3 - 12a^4bmnr^2 + 2a^4bnr^3 - 14a^3bmn^4 \\
& - 24a^3bmn^2r^2 - 2a^3bmr^4 + 8a^3bn^2r^3 \\
& - 8a^2bmn^5 - 12a^2bmn^3r^2 \\
& - 2a^2bn^5r + 2a^2bn^3r^3 - 2abmn^6 - 20abmn^4r^2 \\
& - 2abmn^2r^4 - 8abn^6r + 8abn^4r^3 + 2\mathcal{Q}a^4bnr \\
& + 8\mathcal{Q}a^3bn^2r + 2\mathcal{Q}a^2bn^3r + 8\mathcal{Q}abn^4r - a^7 \\
& - 4a^6n + 2a^5mr - a^5n^2 - a^5r^2 + 8a^4mnr \\
& - 4a^4n^3 - 4a^4nr^2 \\
& + 4a^3mn^2r + a^3n^4 - 2a^3n^2r^2 + 16a^2mn^3r \\
& + 4a^2n^5 - 8a^2n^3r^2 + 2amn^4r + an^6 - an^4r^2 \\
& + 8mn^5r + 4n^7 \\
& - 4n^5r^2 - a^5\mathcal{Q} - 4\mathcal{Q}a^4n - 2\mathcal{Q}a^3n^2 \\
& - 8\mathcal{Q}a^2n^3 - \mathcal{Q}an^4 - 4\mathcal{Q}n^5 \Big),
\end{aligned} \tag{A.7}
$$

$$
\begin{aligned}
f_1 = {} & 2a^9b^2n + 9a^8b^2n^2 - a^8b^2r^2 + 14a^7b^2n^3 \\
& + 4a^7b^2nr^2 + 2a^6b^2mr^3 + 5a^6b^2n^4 \\
& + 16a^6b^2n^2r^2 - a^6b^2r^4 \\
& - 10a^5b^2n^5 + 4a^5b^2n^3r^2 + 2a^5b^2nr^4 \\
& - 10a^4b^2mn^2r^3 - 13a^4b^2n^6 - 17a^4b^2n^4r^2 \\
& + 6a^4b^2n^2r^4 - 6a^3b^2n^7 \\
& - 8a^3b^2n^5r^2 - 2a^3b^2n^3r^4 + 8a^2b^2mn^4r^3 \\
& - a^2b^2n^8 + 2a^2b^2n^6r^2 - 5a^2b^2n^4r^4 \\
& + 2\mathcal{Q}a^7b^2n + 9a^6b^2n^2\mathcal{Q} \\
& - a^6b^2\mathcal{Q}r^2 + 16a^5b^2n^3\mathcal{Q} + 4a^5b^2n\mathcal{Q}r^2 \\
& + 14a^4b^2n^4\mathcal{Q} + 15a^4b^2n^2\mathcal{Q}r^2 + 6a^3b^2n^5\mathcal{Q} \\
& + 8a^3b^2n^3\mathcal{Q}r^2 \\
& + 2\mathcal{Q}a^3b^2nr^4 + a^2b^2n^6\mathcal{Q} - 2a^2b^2n^4\mathcal{Q}r^2 \\
& + a^2b^2n^2\mathcal{Q}r^4 - 2a^8bm - 10a^7bmn - 2a^7bnr \\
& - 22a^6bmn^2 \\
& - 4a^6bmr^2 - 30a^5bmn^3 - 8a^5bmnr^2 + 8a^5bn^3r \\
& - 2a^5bnr^3 - 30a^4bmn^4 - 16a^4bmn^2r^2 - 2a^4bmr^4 \\
& - 22a^3bmn^5 - 28a^3bmn^3r^2 - 2a^3bmnr^4 \\
& + 2a^3bn^5r + 6a^3bn^3r^3 - 10a^2bmn^6 - 12a^2bmn^4r^2 \\
& - 2a^2bmn^2r^4 \\
& - 2abmn^7 - 20abmn^5r^2 - 2abmn^3r^4 - 8abn^7r \\
& + 8abn^5r^3 - 2a^5bn\mathcal{Q}r \\
& + 6a^3bn^3\mathcal{Q}r \\
& + 8abn^5\mathcal{Q}r + 2a^8 \\
& + 4a^7n - 2a^6mr + 5a^6n^2 + 3a^6r^2 + 12a^5n^3 \\
& + 4a^5nr^2 + 4a^4mn^2r + 9a^4n^4 + 4a^4n^2r^2 + a^4r^4 \\
& + 12a^3n^5 + 8a^3n^3r^2 + 14a^2mn^4r + 11a^2n^6 \\
& - a^2n^4r^2 + 2a^2n^2r^4 + 4an^7 + 4an^5r^2 + 8mn^6r \\
& + 5n^8 - 2n^6r^2 + n^4r^4 + a^6\mathcal{Q} - 2a^4n^2\mathcal{Q} \\
& - 7a^2n^4\mathcal{Q} - 4n^6\mathcal{Q},
\end{aligned} \tag{A.8}
$$

and

$$
\begin{aligned}
f_0 = {} & a^8b^2n^2 - a^8b^2r^2 + 4a^7b^2n^3 - 4a^7b^2nr^2 \\
& + 2a^6b^2mr^3 + 5a^6b^2n^4 - a^6b^2r^4 + 8a^5b^2mnr^3 \\
& + 12a^5b^2n^3r^2 - 4a^5b^2nr^4 + 6a^4b^2mn^2r^3 \\
& - 5a^4b^2n^6 + 7a^4b^2n^4r^2 - 2a^4b^2n^2r^4 - 8a^3b^2mn^3r^3 \\
& - 4a^3b^2n^7 - 8a^3b^2n^5r^2 + 4a^3b^2n^3r^4 \\
& - 8a^2b^2mn^4r^3 - a^2b^2n^8 - 6a^2b^2n^6r^2 + 3a^2b^2n^4r^4 \\
& + a^6b^2n^2\mathcal{Q} - a^6b^2\mathcal{Q}r^2 \\
& + 4a^5b^2n^3\mathcal{Q} - 4a^5b^2n\mathcal{Q}r^2 + 6a^4b^2n^4\mathcal{Q} \\
& - a^4b^2n^2\mathcal{Q}r^2 + 4a^3b^2n^5\mathcal{Q} + 8a^3b^2n^3\mathcal{Q}r^2 \\
& + a^2b^2n^6\mathcal{Q} \\
& + 6a^2b^2n^4\mathcal{Q}r^2 + a^2b^2n^2\mathcal{Q}r^4 - 2a^7bmn \\
& - 2a^7bnr - 8a^6bmn^2 - 8a^6bn^2r - 14a^5bmn^3 \\
& - 8a^5bn^3r - 2a^5bnr^3 \\
& - 16a^4bmn^4 + 8a^4bmn^2r^2 - 8a^4bn^2r^3 \\
& - 14a^3bmn^5 + 12a^3bmn^3r^2 - 2a^3bmnr^4 \\
& + 2a^3bn^5r - 10a^3bn^3r^3 \\
& - 8a^2bmn^6 + 8a^2bmn^4r^2 + 8a^2bn^6r \\
& - 8a^2bn^4r^3 - 2abmn^7 + 12abmn^5r^2 - 2abmn^3r^4 \\
& + 8abn^7r - 8abn^5r^3 \\
& - 2a^5bn\mathcal{Q}r - 8a^4bn^2\mathcal{Q}r - 10a^3bn^3\mathcal{Q}r \\
& - 8a^2bn^4\mathcal{Q}r - 8abn^5\mathcal{Q}r + 2a^8 + 8a^7n - 2a^6mr \\
& + 13a^6n^2 \\
& + 3a^6r^2 \\
& - 8a^5mnr + 16a^5n^3 + 8a^5nr^2 - 12a^4mn^2r \\
& + 17a^4n^4 + 12a^4n^2r^2 + a^4r^4 - 16a^3mn^3r \\
& + 8a^3n^5 + 16a^3n^3r^2 \\
& - 18a^2mn^4r + 3a^2n^6 + 15a^2n^4r^2 + 2a^2n^2r^4 \\
& - 8amn^5r + 8an^5r^2 - 8mn^6r - 3n^8 + 6n^6r^2
\end{aligned}
$$

$$+n^4r^4 + a^6\mathcal{Q} + 4\,a^5n\mathcal{Q} + 6\,a^4n^2\mathcal{Q} + 8\,a^3n^3\mathcal{Q} \\ +9\,a^2n^4\mathcal{Q} + 4\,an^5\mathcal{Q} + 4\,n^6\mathcal{Q}. \tag{A.9}$$

Note that the inner radius r_- and outer one r_+ appear in these expressions are the ones correspond to black hole with tidal charge, i.e. $r_\pm = m \pm \sqrt{m^2 + n^2 - a^2 - \mathcal{Q}}$

References

1. M. Astorino, Phys. Lett. B **760**, 393 (2016)
2. M. Appels, R. Gregory, D. Kubiznak, Phys. Rev. Lett. **117**(13), 131303 (2016)
3. M. Appels, R. Gregory, D. Kubiznak, JHEP **1705**, 116 (2017)
4. M. Astorino, Thermodynamics of regular accelerating black holes. Phys. Rev. D **95**(6), 064007 (2017)
5. A. Anabalón, M. Appels, R. Gregory, D. Kubizňák, R.B. Mann, A. Ovgün, Phys. Rev. D **98**(10), 104038 (2018)
6. J. Podolsky, A. Vratny, Phys. Rev. D **102**(8), 084024 (2020)
7. J. Podolsky, A. Vratny, Phys. Rev. D **104**, 084078 (2021)
8. J. Podolsky, A. Vratny, Phys. Rev. D **107**(8), 084034 (2023)
9. J. Barrientos, A. Cisterna, Phys. Rev. D **108**(2), 024059 (2023)
10. H.M. Siahaan, Phys. Lett. B **782**, 594–601 (2018)
11. J. Barrientos, A. Cisterna, K. Pallikaris, Gen. Relativ. Gravit. **56**(9), 111 (2024)
12. P.V.P. Cunha, C.A.R. Herdeiro, E. Radu, H.F. Runarsson, Phys. Rev. Lett. **115**(21), 211102 (2015)
13. A. Grenzebach, V. Perlick, C. Lämmerzahl, Phys. Rev. D **89**(12), 124004 (2014)
14. P.C. Li, M. Guo, B. Chen, Phys. Rev. D **101**(8), 084041 (2020)
15. S.W. Wei, Y.C. Zou, Y.X. Liu, R.B. Mann, JCAP **08**, 030 (2019)
16. H.M. Wang, Y.M. Xu, S.W. Wei, JCAP **03**, 046 (2019)
17. M. Zhang, J. Jiang, Phys. Rev. D **103**(2), 025005 (2021)
18. A. Ashoorioon, M.B. Jahani Poshteh, R.B. Mann, Phys. Rev. D **107**(4), 044031 (2023)
19. T.C. Frost, V. Perlick, Class. Quantum Gravity **38**(8), 085016 (2021)
20. J.B. Griffiths, J. Podolsky, *Exact Space-Times in Einstein's General Relativity* (Cambridge University Press, Cambridge, 2009)
21. A. Kumar, D.V. Singh, S. Upadhyay, Int. J. Mod. Phys. A **39**(31), 2450136 (2024)
22. S.U. Islam, S.G. Ghosh, S.D. Maharaj, JCAP **12**, 047 (2024)
23. M. Ghasemi-Nodehi, Universe **10**(9), 378 (2024)
24. X.J. Gao, Eur. Phys. J. C **84**(9), 973 (2024)
25. W. Liu, D. Wu, J. Wang, Phys. Lett. B **858**, 139052 (2024)
26. J.F. Plebanski, M. Demianski, Ann. Phys. **98**, 98–127 (1976)
27. H.M. Siahaan, Nucl. Phys. B **1008**, 116704 (2024)
28. H.M. Siahaan, Eur. Phys. J. C **84**(10), 1069 (2024)
29. H.M. Siahaan, Phys. Rev. D **102**(6), 064022 (2020)
30. N. Dadhich, R. Maartens, P. Papadopoulos, V. Rezania, Phys. Lett. B **487**, 1–6 (2000)
31. A.N. Aliev, A.E. Gumrukcuoglu, Phys. Rev. D **71**, 104027 (2005)
32. A.N. Aliev, H. Cebeci, T. Dereli, Phys. Rev. D **77**, 124022 (2008)
33. A.N. Aliev, A.E. Gumrukcuoglu, Class. Quantum Gravity **21**, 5081–5096 (2004)
34. K. Hioki, K.I. Maeda, Phys. Rev. D **80**, 024042 (2009)
35. P.V.P. Cunha, C.A.R. Herdeiro, E. Radu, H.F. Runarsson, Int. J. Mod. Phys. D **25**(09), 1641021 (2016)
36. A. Abdujabbarov, F. Atamurotov, Y. Kucukakca, B. Ahmedov, U. Camci, Astrophys. Space Sci. **344**, 429–435 (2013)
37. L. Randall, R. Sundrum, Phys. Rev. Lett. **83**, 4690–4693 (1999)
38. T. Shiromizu, K.I. Maeda, M. Sasaki, Phys. Rev. D **62**, 024012 (2000)
39. N. Dadhich, R. Maartens, P. Papadopoulos, V. Rezania, Phys. Lett. B **487**, 1 (2000)
40. A. Chamblin, H.S. Reall, H.A. Shinkai, T. Shiromizu, Phys. Rev. D **63**, 064015 (2001)
41. J.C.S. Neves, C. Molina, Phys. Rev. D **86**, 124047 (2012)
42. M. Zhang, J. Jiang, Phys. Lett. B **816**, 136213 (2021)
43. K. Akiyama et al. [Event Horizon Telescope], Astrophys. J. Lett. **875**, L1 (2019)
44. K. Akiyama et al. [Event Horizon Telescope], Astrophys. J. Lett. **930**(2), L12